McMaster University

Advanced Optimization Laboratory

Title:

An Optimal Nearly-Analytic Discrete Method for 2D Acoustic and Elastic Wave Equations

Authors:

Dinghui Yang, Ming Lu, Rushan Wu and Jiming Peng

AdvOl-Report No. 2004/9

July 2004, Hamilton, Ontario, Canada

An Optimal Nearly-Analytic Discrete Method for 2D Acoustic and Elastic Wave Equations

Dinghui Yang[1] and Ming Lu[1]
[1]Department of Mathematical Sciences, Tsinghua University, Beijing 100084, P. R. China
(dhyang@math.tsinghua.edu.cn)

Rushan Wu[2]
[2]Institute of Tectonics, University of California, Santa Cruz, CA 95064, USA
(rwu@es.ucsc.edu)

Jiming Peng[3]
[3]Department of Computing and Software, McMaster Univeristy, Hamilton, Canada
(pengj@mcmster.ca)

Bulletin of the Seismological Society of America (in press)

Abstract

In this article, we present the so-called optimal nearly-analytic discrete method (ONADM), which is an improved version of the NADM proposed recently in BSSA (Yang, et al., 2003a). We compare numerically the error of the ONADM with those of the NADM and other FD methods for 1D and 2D cases, and give the wave-field modeling in 2-D isotropic media. We also discuss the validity of the n-times absorbing boundary condition (ABC) when the absorbing boundary conditions are incorporated in ONADM. We show that, compared with the original NADM, the ONADM for the 2-D case can reduce significantly the storage space and computational cost. The time accuracy of the optimal method is also increased from 2-order of the original NADM to 4-order while the space accuracy remains the same as that of the original one. Promising numerical results suggest that the ONADM is suitable for large-scale numerical modeling as it can suppress effectively numerical dispersions caused by discretizing the wave equations when too-coarse grids are used.

Introduction

Analysis of seismic data to determine earth structure and seismic source parameters requires accurate and efficient methods for computing synthetic seismograms. When it is hard to solve the wave equations, we usually refer to two kinds of approximate methods. One approximate method is the perturbation method and the other is the discretization method in which we first discretize the wave equations and then solve the resulting finite-difference equations.

Time-domain methods discretize the spatial and temporal derivatives in acoustic and elastic wave equations. Several widely used methods such as second-order center scheme (Alford, et al., 1974; Kelly, et al., 1976; Igel, et al., 1995) and various high-order compact schemes or so-called Lax-Wendroff scheme (Dablain, 1986; Blanch and Robertsson, 1997; Wang et al., 2002) are based on the finite-difference (FD) method. There are also other methods that use the pseudo-spectral (PS) method to compute spatial derivatives (e.g. Kosloff and Baysal, 1982).

FD methods have been proven to be successful and provided useful tools for exploring seismology. Due to this reason, numerous finite-difference schemes have been widely employed to solve acoustic and elastic wave equations (Alford, et al., 1974; Kelly, et al., 1976; Dablain, 1986; Virieux, 1986; Takeuchi and Geller, 2000; others). These FD methods are also applied to anisotropic and viscoelastic problems (Robertsson, et al., 1994; Igel, et al., 1995; Blanch and Robertsson, 1997; Zhang, et al., 1999; Takeuchi and Geller, 2000). However, it should be mentioned that some FD methods like the conventional finite-difference methods with 2- and 4-orders often suffer from seriously numerical dispersion when too few samples per wavelength are used or when the models have large velocity contrast, or artifacts caused by source at grid points (Fei and Larner, 1995; Yang, et al., 2002). Numerical dispersions affect not only the performance of the lower-order FD methods, but also the performance of the so-called high-order FD methods. For example, the 10-order compact FD schemes (e.g. Wang, et al., 2002), which

usually use more grids than low-order schemes, also suffer from numerical dispersions. The demand of more grids in high-order FD methods prevents the algorithms from efficient parallel implementation and artificial boundary treatment. On the other hand, although the numerical dispersions or undesirable ripples can also be suppressed using the so-called flux-corrected transport (FCT) technique, the FCT method is typically unable to fully recover the lost resolution by the numerical dispersion when the spatial sampling becomes too coarse (Yang, et al., 2002). The pseudo-spectral method (Kosloff and Baysal, 1982) is attractive as the space operators are exact up to the Nyquist frequency, but it requires the Fourier transform of wave-field to be made, which is computationally expensive for 3-D anisotropic models and has difficulty in handing sharp boundaries (Mizutani et al., 2000). Moreover, taking the Fourier transform means that each point interacts with every other point. To some extent, this is inconsistent with the physical phenomena as interaction in dynamic elasticity is of a local nature.

Recently, Yang developed a perturbation method, called “nearly analytic discrete method (NADM)” for acoustic and elastic equations (Yang, et al., 2003a). The NADM was initially suggested by Konddoh et al.(1994) for solving parabolic and hyperbolic equations. The method, based on the so-called “thought analysis” criterion (Konddoh et al., 1994), uses a truncated Taylor expansion with respect to time to analytically approximate the wave displacement and its first-order partial derivatives at grid-points. Then it uses some interpolation relations based on the function of the truncated Taylor expansion with respect to spatial increments to determine the high-order space derivatives involved in these truncated Taylor formulae. On the basis of such a structure, the method enables effectively to suppress the numerical dispersion caused by discretizing the wave equation by using the local interpolation compensation for the truncated Taylor series, while the conventional FD schemes suffer from numerical dispersion near large velocity contrast or when too few samples per wavelength are used (Yang, et al., 2003a). Further, by using the first-order spatial derivatives and the wave displacement simultaneously, we can determine high-order spatial derivatives based on the interpolation relations that can be explicitly handled. This is different from other FD methods that use a discrete expression to approximate the original wave equation. In the following sections, we shall further discuss the difference between the NADM and Lax-Wendroff/compact/optimal FD methods.

The main purpose of this paper is to discuss the efficient implementation of the NADM. For this we present a modified version of NADM, called optimal NADM (or ONADM in brief). Our theoretical analyses shows that the ONADM can improve significantly over the original one in numerous perspectives including numerical errors, storage spaces, and computational cost. The accuracy of the ONAMD in time also increases from 2-order of the original NADM to 4-order. Promising numerical results verify our theoretical conclusions. Meanwhile, we also discuss the validity of the n-times absorbing boundary condition, developed in the cited references (Higdon, 1991; Yang, et al., 2003b).

Basic Nearly Analytic Discrete Method

To illustrate the derivation of the NADM, we briefly review and summarize the key

ideas in it. For the 2-D case, the wave equation can be written as

$$\frac{\partial \sigma_{ij}}{\partial x_j} + f_i = \rho \frac{\partial^2 u_i}{\partial t^2}, \quad i=1,2,3, \qquad (1)$$

where subscript j takes the values of 1 and 3, $\rho = \rho(x,z)$ is the medium density, u_i denotes the displacement component in the ith direction, f_i is the force-source component in the ith direction, and σ is the stress tensor.

We use the same notation as that in the original NADM (Yang, et al., 2003a), i.e.

$$U = \left(u_x, u_y, u_z\right)^T, \quad \frac{\partial^2 U}{\partial t^2} \equiv P,$$

$$\overline{U} = \left[U, \frac{\partial U}{\partial x}, \frac{\partial U}{\partial z}\right]^T, \quad \overline{P} = \left[P, \frac{\partial P}{\partial x}, \frac{\partial P}{\partial z}\right]^T, \text{ and } \overline{W} = \frac{\partial}{\partial t}\overline{U}.$$

Note that $\overline{W}$ is the time derivative of both the displacement component U and its first-order spatial derivatives, which is called simply the velocity $\overline{W}$. Using the above notation with values at the time t_n and the truncated Taylor series expansion, Yang, et al. (2003a) obtained the following formulae

$$\overline{U}_{i,j}^{n+1} = \overline{U}_{i,j}^{n} + \Delta t \overline{W}_{i,j}^{n} + \frac{(\Delta t)^2}{2}\overline{P}_{i,j}^{n} + \frac{(\Delta t)^3}{6}\left(\frac{\partial \overline{P}}{\partial t}\right)_{i,j}^{n} + \frac{(\Delta t)^4}{24}\left(\frac{\partial^2 \overline{P}}{\partial t^2}\right)_{i,j}^{n}, \qquad (2)$$

$$\overline{W}_{i,j}^{n+1} = \overline{W}_{i,j}^{n} + \Delta t \overline{P}_{i,j}^{n} + \frac{(\Delta t)^2}{2}(\frac{\partial \overline{P}}{\partial t})_{i,j}^{n} + \frac{(\Delta t)^3}{6}(\frac{\partial^2 \overline{P}}{\partial t^2})_{i,j}^{n}, \qquad (3)$$

where Δt denotes the time increment.

Obviously, the more the series terms $\left(\frac{\partial^k \overline{P}}{\partial t^k}\right)_{i,j}^{n}$ $(k = 0,1,2,\cdots)$ are kept in formulae (2) and (3), the more accuracy the computed values of $\overline{U}_{i,j}^{n+1}$ and $\overline{W}_{i,j}^{n+1}$ are. Unfortunately, it is impossible to use the infinite Taylor series expansion. As an alternative, we use the truncated Taylor series expansions (2) and (3) that have lower computational accuracy regarding $\overline{U}_{i,j}^{n+1}$ and $\overline{W}_{i,j}^{n+1}$ because of the loss of the seismic information included in the higher-order terms in the Taylor series. To capture these lost seismic information and further increase the computational accuracy, according to the "analysis thought" (Konddoh et al., 1994), we can approximately incorporate the lost information by introducing the interpolation function and using the connection relations. In order to achieve this target and avoid the implicit schemes and costing storage derived from direct

central-differencing of the high-order time derivatives of $\overline{U}$ that included implicitly in $\left(\frac{\partial^k \overline{P}}{\partial t^k}\right)$(k=1,2) (equations (2) and (3)), we convert these high-order time derivatives to the spatial derivatives $\left(\frac{\partial^{k+l} U}{\partial x^k \partial z^l}\right)_{i,j}^n \quad (2 \le k+l \le 5)$ for equations (2) and (3) and $\left(\frac{\partial^{k+l} \overline{W}}{\partial x^k \partial z^l}\right)_{i,j}^n$ $(2 \le k+l \le 3)$ for equation (3). The transform used here is similar to the high-order FD methods (Dablain, 1986) or the so-called Lax-Wendroff correction (LWC) methods (Blanch and Robertsson, 1997). However, the way that the NADM approximates the high-order spatial derivatives is completely different from the later ones. It is also different from the optimal FD scheme based on a predictor-corrector method (Geller and Takeuchi, 1998; Takeuchi and Geller, 2000). The high-order FD methods (Dablain, 1986) (or the so-called LWC) uses only the wave displacement to determine the high-order spatial derivatives while the NADM uses both the wave displacement and its gradients to determine the high-order spatial derivatives. Compared with high-order FD schemes, the NADM needs fewer grids to achieve the same accuracy. For example, the NADM using 3 grid points in a direction has 4-order space accuracy, the same as that of the high-order compact FD scheme (Dablain, 1986; Wang, et al., 2002) with 5 grids. To be more specific, let us consider the NADM based on the Taylor series expansion on variables X and Z. We use the following interpolation function

$$G(X,Z) = \sum_{r=0}^{M} \frac{1}{r!} \left(X \frac{\partial}{\partial x} + Z \frac{\partial}{\partial z}\right)^r U \,. \tag{4}$$

To determine the high-order spatial derivatives, we use formulae (4) at the grid point (i, j) and its eight neighboring nodes: (i-1, j), (i+1, j), (i, j-1), (i, j+1), (i-1, j-1), (i-1, j+1), (i+1, j-1), and (i+1, j+1). Let us take the grid point (i-1, j) as an illustrating example for the interpolation relations, we have

$$\begin{aligned} &\left[G(-\Delta x,0)\right]_{i,j}^n = U_{i-1,j}^n, \\ &\left[\frac{\partial}{\partial X} G(-\Delta x,0)\right]_{i,j}^n = \left(\frac{\partial}{\partial x} U\right)_{i-1,j}^n, \quad \text{and} \\ &\left[\frac{\partial}{\partial Z} G(-\Delta x,0)\right]_{i,j}^n = \left(\frac{\partial}{\partial z} U\right)_{i-1,j}^n, \end{aligned} \tag{5}$$

where Δx is the spatial increment in the x-axis direction. From these relations, we can find the analytic expressions of $\left(\frac{\partial^{k+l} U}{\partial x^k \partial z^l}\right)_{i,j}^n \quad (2 \le k+l \le 5)$ in terms of the displacement U and its first-order spatial partial derivatives at the mesh point (i, j) and its neighboring

grids (Yang, et al., 2003a).

Following the above-mentioned scheme, when computing $U_{i,j}^{n+1}$, the NADM uses not only the values of the displacement U at the mesh point (*i*, *j*) and its neighboring grid points, but also the values of the partial derivatives of U with respect to time *t* and space *x*, *z* (see equations (2) and (3)). This allows the algorithm to capture more seismic information in both the function U^n and its partial derivatives. Therefore, the NADM can effectively suppress the loss of information included in the higher-order terms of the Taylor expansion, further resulting in great numerical accuracy and less numerical dispersions. The introduction of the local connection relations (5) greatly improves the continuity and derivability of the approximate function U^n (because U^n is an approximate variable during data processing) and consequently stabilizes the NADM.

Optimal Nearly-Analytic Discrete Method

Now let us take a closer look at formula (2) in the NADM. To compute the velocity $\overline{W}_{i,j}^{n}$ at the grid-point (*i*, *j*) in formula (3) that is necessary for computing $\overline{U}_{i,j}^{n+1}$, we have to calculate $\left(\frac{\partial^{k+l}\overline{W}}{\partial x^k \partial z^l}\right)_{i,j}^{n}$ $(2 \le k+l \le 3)$ because of the involvement of the higher-order partial derivatives in formula (3). In our earlier work (Yang, et al., 2003a), the velocity $\overline{W}$ is calculated by using the following backward difference method:

$$\left(\frac{\partial^{k+l}\overline{W}}{\partial x^k \partial z^l}\right)_{i,j}^{n} = \left[\left(\frac{\partial^{k+l}\overline{U}}{\partial x^k \partial z^l}\right)_{i,j}^{n} - \left(\frac{\partial^{k+l}\overline{U}}{\partial x^k \partial z^l}\right)_{i,j}^{n-1}\right] \Big/ \Delta t, \quad 2 \le k+l \le 3 \tag{6}$$

This leads to several disadvantages: (1) additional computational cost for computing $\overline{W}_{i,j}^{n}$; (2) lower time accuracy because of the use of low-order difference scheme (6), which is only 2-order in time while the space accuracy is 4-order for the NADM (Yang, et al., 2003a); (3) higher storage requirement. For example, we introduce a new vector $\overline{U}$ with 9 components and thus we need 18 arrays to store $\overline{U}_{i,j}^{n+1}$ and $\overline{U}_{i,j}^{n}$. Since $\overline{W} = \partial\overline{U}/\partial t$, we also need 18 arrays to store $\overline{W}_{i,j}^{n+1}$ and $\overline{W}_{i,j}^{n}$. Storing $\left(\frac{\partial^{k+l}U}{\partial x^k \partial z^l}\right)_{i,j}^{n-1}$ $(2 \le k+l \le 3)$ requires 21 arrays and thus we need 39 arrays to store all the information for computing $\left(\frac{\partial^{k+l}\overline{W}}{\partial x^k \partial z^l}\right)_{i,j}^{n}$ $(2 \le k+l \le 3)$. Therefore, the number of total arrays involved in NADM is 57.

In order to improve the original NADM regarding the above-mentioned points, we try to reduce the additional computational cost and storage for computing the velocity

$\overline{W}_{i,j}^{n}$. Actually, by using the values at time t_n and the Taylor series expansion, we can obtain the approximate solution of $\overline{U}_{i,j}^{n-1}$ at time t_{n-1} as follows:

$$\overline{U}_{i,j}^{n-1} = \overline{U}_{i,j}^{n} - \Delta t \overline{W}_{i,j}^{n} + \frac{(\Delta t)^2}{2}\overline{P}_{i,j}^{n} - \frac{(\Delta t)^3}{6}\left(\frac{\partial \overline{P}}{\partial t}\right)_{i,j}^{n} + \frac{(\Delta t)^4}{24}\left(\frac{\partial^2 \overline{P}}{\partial t^2}\right)_{i,j}^{n}. \quad (7)$$

Adding equation (7) and equation (2) together, we obtain the following formula:

$$\overline{U}_{i,j}^{n+1} = 2\overline{U}_{i,j}^{n} - \overline{U}_{i,j}^{n-1} + (\Delta t)^2 \overline{P}_{i,j}^{n} + \frac{(\Delta t)^4}{12}\left(\frac{\partial^2 \overline{P}}{\partial t^2}\right)_{i,j}^{n}. \quad (8)$$

Because both $\overline{P}$ and $\frac{\partial^2 \overline{P}}{\partial t^2}$ can be expressed via $\overline{U}$ and its partial derivatives $\frac{\partial^{k+l}\overline{U}}{\partial x^k \partial z^l}$ (Yang, et al., 2003a), the optimal formula (8) does not involve the velocity $\overline{W}_{i,j}^{n}$. This indicates that if we use formula (8) to compute $\overline{U}_{i,j}^{n+1}$, we do not need to compute both $\overline{W}_{i,j}^{n}$ and $\left(\frac{\partial \overline{P}}{\partial t}\right)_{i,j}^{n}$, thus the storage for $\overline{W}_{i,j}^{n+1}$, $\overline{W}_{i,j}^{n}$, and $\left(\frac{\partial^{k+l} U}{\partial x^k \partial z^l}\right)_{i,j}^{n-1}$ $(2 \le k+l \le 3)$ can also be waived. The introduction of the optimal algorithm (8) reduces significantly the computational cost and storages without sacrificing the accuracy, as the ONADM involves only $\overline{U}_{i,j}^{n+1}$, $\overline{U}_{i,j}^{n-1}$, and $\overline{U}_{i,j}^{n}$. As a consequence, the number of total arrays required for computation in the ONADM reduces to 27 while the original NADM requires 57 arrays as stated earlier. This saves the storage space roughly 53 percent compared with the original one for the 2-D homogeneous case. Meanwhile, the time accuracy increases from 2-order of the original NADM to 4-order because there is no need to compute the derivative $\left(\frac{\partial^{k+l}\overline{W}}{\partial x^k \partial z^l}\right)_{i,j}^{n}$ in the optimal formula (8). Moreover, the ONADM enjoys the same space accuracy as the NADM does, as shown in the error analysis in the cited reference (Yang et al., 2003a) and formula (8).

From formula (8), we can find that the optimal method is quite similar to the so-called Lax-Wendroff or compact schemes or high-order optimal FD schemes, where the original wave equation is used to convert the high-order error terms in Taylor expansions to spatial derivatives that can be handled explicitly thereby increasing the accuracy of the method significantly (Dablain, 1986; Blanch and Robertsson, 1997; Takeuchi and Geller, 2000). However, the ONADM and the NADM are different from

the above-mentioned methods in the ways of approximating the higher-order spatial derivatives. Both the ONADM and the NADM use the displacement and its gradients to determine the high-order spatial derivatives, while the above high-order FD methods use only the wave displacement to determine the high-order spatial derivatives and thus hard to capture the seismic information characterized by the gradient of wave displacement.

In the ONADM, we also employ the truncated Taylor series function (4) of spatial increments and the connection relation (5) to determine the high-order spatial derivatives at the grid-point (*i, j*), the same technique as we used in the original NADM. Therefore, the ONADM enjoy several desirable properties as the original NADM. It can suppress effectively the loss of seismic information included in the higher-order terms of the infinite Taylor expansion, leading to great numerical accuracy and less numerical dispersions as verified by our numerical experiments. Moreover, as shown in our earlier analysis, the ONADM is much more efficient in computation than the NADM as the computational cost and storage requirement in the ONADM is much less than that in the NADM, while the time accuracy is improved from 2-order to 4-order.

Absorbing Boundary Conditions

Due to the limitation in computational source, the computational domain is artificially restricted in the numerical modeling of acoustic and elastic waves propagating in unbounded media. This results in unphysical reflections derived from the artificial boundaries. As a remedy for this issue, absorbing boundary conditions (ABCs) are developed and widely used in the numerical simulations of wave motions in unbounded media to reduce the spurious numerical reflections. In what follows we discuss the issue of how to eliminate spurious reflections from artificial boundaries in the ONADM for simulating seismic propagation in an unbounded domain. For this, we first need to choose a suitable ABC to treat with the boundary reflections. Among the methods developed, the perfectly matched layer (PML) technique, originally used in the electromagnetic wave equation, is recently applied popularly in acoustic and elastic wave simulations (Chew and Liu, 1996; Liu and Tao, 1997). The PML technique, although successful in many applications as a material ABC, requires some special treatments such as the stretched coordinate transformation and/or splitting the velocity field and introducing some new variables for the elastic wave case, while the decoupled ABC does not require to introduce new variables and to do special treatments. Therefore, we choose the following decoupled ABC at the boundary x=0 (Higdon, 1991) that is implemented using the stable biased-center scheme presented in the cited reference (Yang, et al., 2003b),

$$\prod_{i=1}^{n}\left(\frac{\partial}{\partial t}-\frac{v}{\cos\theta_i}\frac{\partial}{\partial x}\right)u\Big|_{x=0}=0, \tag{9}$$

where v is the wave velocity , θ_i $(0\le\theta_i<\pi/2)$ is the incident angle, n denotes absorbing times.

Numerical Errors

1-D case

To test the accuracy of numerical results, we first choose the following 1-D initial problem:

$$\frac{\partial^2 u}{\partial x^2} = \frac{1}{\alpha^2}\frac{\partial^2 u}{\partial t^2}, \tag{10a}$$

$$u(0,x) = \cos(-\frac{2\pi f}{\alpha}\cdot x), \text{ and} \tag{10b}$$

$$\frac{\partial u(0,x)}{\partial t} = -2\pi f \cdot \sin(-\frac{2\pi f}{\alpha}\cdot x), \tag{10c}$$

where *f* denotes the frequency and α is the wave velocity.

Obviously, the analytical solution for the initial problem (10) is

$$u(t,x) = \cos\left[2\pi f\,(t-\frac{x}{\alpha})\right].$$

For comparison, we use the so-called LWC (fourth-order compact scheme (Dablain, 1986)) for equation (10).

In our calculation, the parameters are chosen in the following way. The grid number N=200, the frequency f=15 Hz, and the wave velocity $\alpha = 4000$ m/sec. The relative error (E_r) is the ratio of the RMS of the residual $(u_i^n - u(t_n, x_i))$ and the RMS of the exact solution $u(t_n, x_i)$. Its explicit definition is as follows:

$$E_r(\%) = \left\{\frac{1}{\sum_{i=1}^{N}[u(t_n,x_i)]^2}\sum_{i=1}^{N}\left[u_i^n - u(t_n,x_i)\right]^2\right\}^{\frac{1}{2}} \times 100. \tag{11}$$

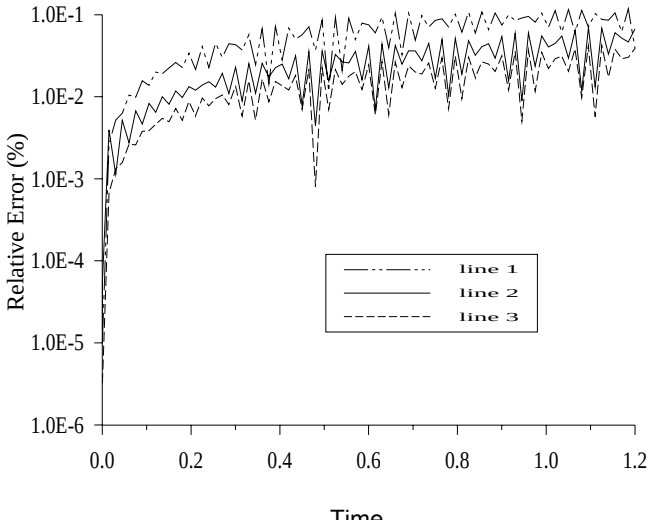

Figure 1. The relative errors of the Lax-Wendroff correction (line 1), the NADM (line 2), and the ONADM (line 3) measured by E_r (formula (11)) are shown in a semi-log scale for the 1-D initial problem (10). The spatial and temporal increments are 10 m and 10^{-4} s, respectively.

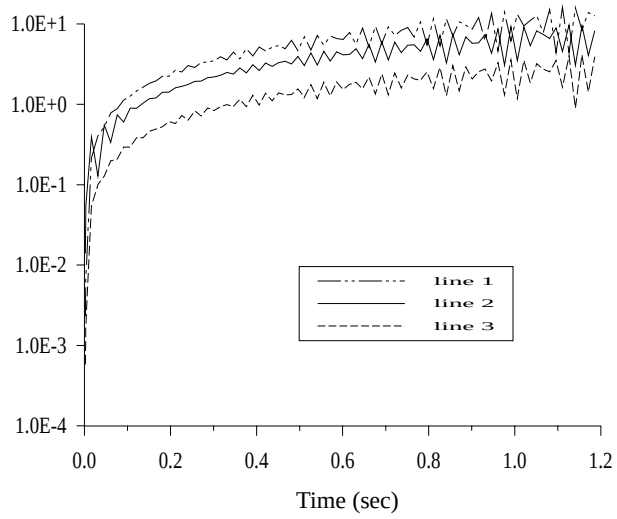

Figure 2. The relative errors of the Lax-Wendroff correction (line 1), the NADM (line 2), and the ONADM (line 3) measured by E_r (formula (11)) are shown in a semi-log scale for the 1-D initial problem (10). The spatial and temporal increments are 30 m and 10^{-3} s, respectively.

Figures 1 and 2 show the computational results of the relative error E_r at different times for cases of different spatial and time increments, where three lines of E_r for the fourth-order LWC (line 1), the NADM (line 2), and the ONADM (line 3) are shown in a semi-log scale. From Figures 1 and 2, we can conclude that the error introduced by the ONADM measured by E_r is less than those of the NADM and the fourth-order LWC. In Figure 1, the maximum E_r of the ONADM is 0.0163% while the maximum relative errors

are 0.0269% for the NADM and 0.0595% for the LWC, respectively. Comparing Figure 2 with Figure 1, we can see that the relative errors increase with the increase of the spatial and time increments. The maximum relative errors shown in Figure 2 are 1.5336%, 3.8665%, and 6.1782% for the ONADM, NADM, and the so-called LWC, respectively.

2-D case

To further compare the accuracy of numerical results, we choose the following 2-D initial problem that is similar to that of the 1-D case:

$$\frac{\partial^2 \mathrm{u}}{\partial \mathrm{x}^2} + \frac{\partial^2 \mathrm{u}}{\partial \mathrm{z}^2} = \frac{1}{\alpha^2}\frac{\partial^2 \mathrm{u}}{\partial \mathrm{t}^2}, \tag{12a}$$

$$u(0,x,z) = \cos(-\frac{2\pi f}{\alpha}\cdot\cos\theta_0\cdot x - \frac{2\pi f}{\alpha}\cdot\sin\theta_0\cdot z), \text{ and} \tag{12b}$$

$$\frac{\partial u(0,x,z)}{\partial t} = -2\pi f\cdot\sin(-\frac{2\pi f}{\alpha}\cdot\cos\theta_0\cdot x - \frac{2\pi f}{\alpha}\cdot\sin\theta_0\cdot z), \tag{12c}$$

where α is the velocity of the plane wave and θ_0 is an incident angle at time $t = 0$. We mention that the analytical solution for the initial problem can be found in the cited reference (Yang, et al., 2003a).

In our numerical experiments, all the parameters are chosen as follows: the grid number N=200, the frequency f=15 Hz, $\alpha = 4000$ m/sec, and $\theta_0 = \pi/4$. The relative error in 2-D case is defined by:

$$E_r(\%) = \left\{ \frac{1}{\sum_{i=1}^{N}\sum_{j=1}^{N}\left[u(t_n,x_i,z_j)\right]^2} \sum_{i=1}^{N}\sum_{j=1}^{N}\left[u_{i,j}^n - u(t_n,x_i,z_j)\right]^2 \right\}^{\frac{1}{2}} \times 100. \tag{13}$$

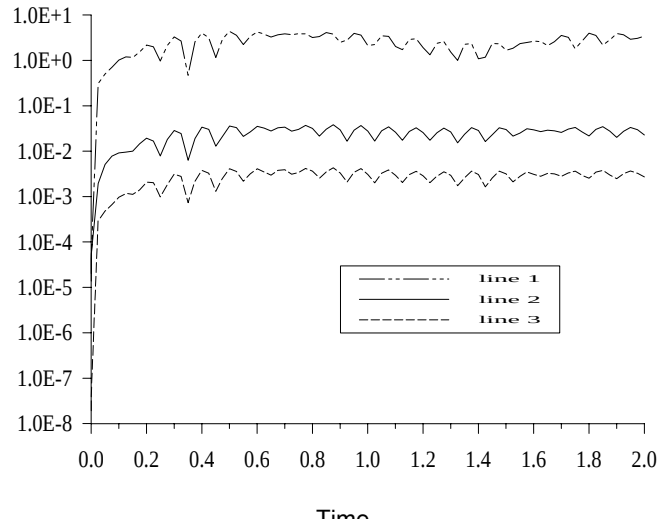

Figure 3. The relative errors of the second-order FD (line 1), the NADM (line 2), and the

ONADM (line 3) measured by E_r are shown in a semi-log scale for the 2-D initial problem (12). The spatial and temporal increments are 10 m and 10^{-4} s, respectively.

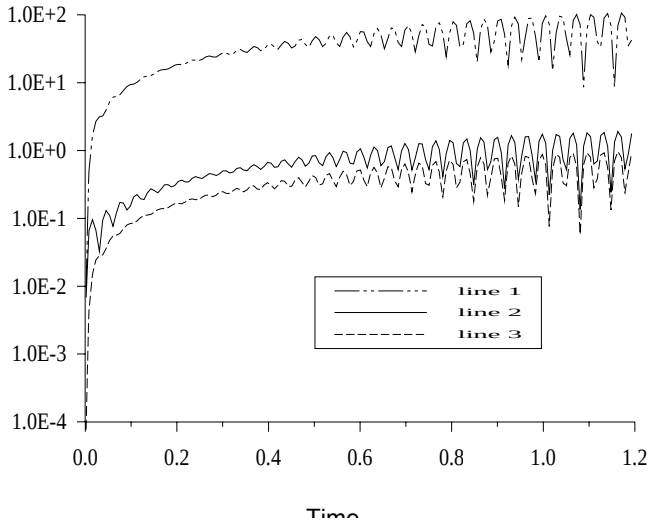

Figure 4. The relative errors of the second-order FD (line 1), the NADM (line 2), and the ONADM (line 3) measured by E_r are shown in a semi-log scale for the 2-D initial problem (12). The spatial and temporal increments are 30 m and $5x10^{-4}$ s, respectively.

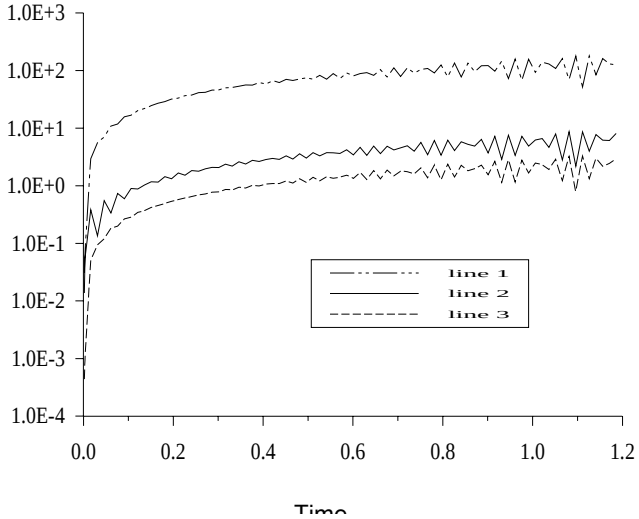

Figure 5. The relative errors of the second-order FD (line 1), the NADM (line 2), and the ONADM (line 3) measured by E_r are shown in a semi-log scale for the 2-D initial problem (12). The spatial and temporal increments are 40 m and 10^{-3} s, respectively.

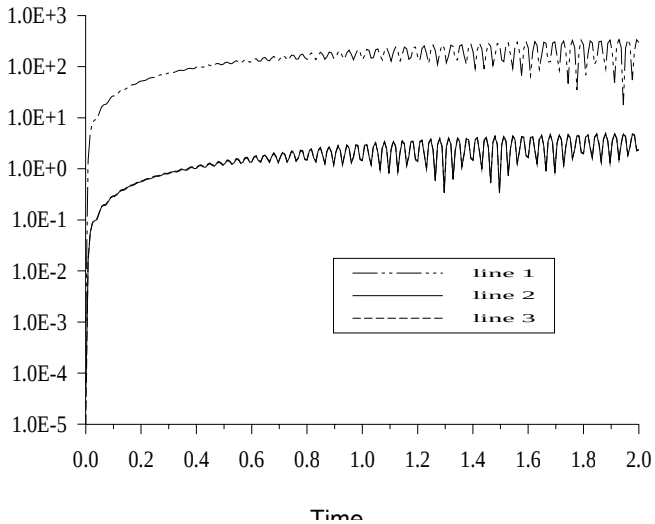

Figure 6. The relative errors of the second-order FD (line 1), the NADM (line 2), and the ONADM (line 3) measured by E_r are shown in a semi-log scale for the 2-D initial problem (12). The spatial and temporal increments are 50 m and 10^{-4} s, respectively.

Table 1. Comparison of maximum E_r (%) for different cases and different methods.

Methods	Second-order FD	NADM	ONADM
Case 1: $h=10m$, $\Delta t=10^{-4}s$	2.5191	0.0243	0.0027
Case 2: $h=30m$, $\Delta t=5\times10^{-4}s$	41.2983	0.7484	0.3758
Case 3: $h=40m$, $\Delta t=10^{-3}s$	76.4788	3.6053	1.3483
Case 4: $h=50m$, $\Delta t=10^{-4}s$	154.127	1.9902	1.9902

Figures 3, 4, 5, and 6 are the curves of the error E_r versus time corresponding to different spatial and time step sizes, where three lines of E_r for the second-order center scheme (line 1), the NADM (line 2), and the ONADM (line 3) are shown in a semi-log scale. In these Figures, the maximum relative errors for different cases are listed in Table 1. From these error curves and Table 1 ($\Delta x=\Delta z=h$), we find that E_r increases corresponding to the increase in the time and/or spatial increments for all the three methods. Figures 3, 4, and 5 show that the ONADM has the highest accuracy among them. It should be noted that Figure 6 presents two identical curves for the case with the same small time increment ($\Delta t=10^{-4}$ s) and the large spatial increment (h=50 m),

computed by the ONADM and the NADM respectively, while the relative error E_r generated by the ONADM is smaller than the error E_r of the NADM for the case 1 with the fine spatial grids and the same time increment as case 4. It shows that for the special case (case 4) the errors of both the ONADM and the NADM depend mainly on the spatial increment. This coincides with the fact that the ONADM and the NADM have the same spatial accuracy. Further, from Figures 3, 4, and 5, the conclusion that the accuracy of the ONADM in time is higher than that of the NADM can be verified as the relative errors of the ONADM are smaller than those of the NADM for cases 1, 2, and 3. Our numerical results are consistent with what we derived in our theoretical analyses.

Wave-Field Modeling

In this section, we compare the isotropic wave-field simulations computed by the NADM and the ONADM. In this case, equation (1) can be specified to

$$\begin{cases} \rho \dfrac{\partial^2 u_x}{\partial t^2} = (\lambda + 2\mu)\dfrac{\partial^2 u_x}{\partial x^2} + \mu \dfrac{\partial^2 u_x}{\partial z^2} + (\lambda + \mu)\dfrac{\partial^2 u_z}{\partial x \partial z} + f_1 & (14a) \\ \rho \dfrac{\partial^2 u_y}{\partial t^2} = \mu\left(\dfrac{\partial^2 u_y}{\partial x^2} + \dfrac{\partial^2 u_y}{\partial z^2}\right) + f_2 & (14b) \\ \rho \dfrac{\partial^2 u_z}{\partial t^2} = (\lambda + \mu)\dfrac{\partial^2 u_x}{\partial x \partial z} + \mu \dfrac{\partial^2 u_z}{\partial x^2} + (\lambda + 2\mu)\dfrac{\partial^2 u_z}{\partial z^2} + f_3 & (14c) \end{cases}$$

where λ and μ are Lamé constants.

In the first model (model 1), we choose λ=2.75 (GPa), μ=6.25 (GPa), and the density $\rho = 2.1 g/cm^3$. The computational domain is $0 \le x \le 9.95$ km, $0 \le z \le 9.95$ km. We choose the spatial increment *h*=50 m, the time increment $\Delta t = 3 \times 10^{-3}$ sec, and the number of grid points 200×200. The source is an explosive source that is at coordinate (x_s, z_s) = (4.95 km, 4.95 km) and has a Ricker wavelet with a peak frequency of f_0=15 Hz. The time variation of the source function is $\sin(2\pi f_0 t)\exp(-4\pi^2 f_0^2 t^2/16)$ (Zahradnik, et al., 1993).

Figures 7 and 8 are the wave-field snapshots at t= 1.4 sec generated by the original NADM and the ONADM, respectively. From the three-component snapshots, we can see that these two wave-field results are identical, and the P- and SV-waves presented in the horizontal component u_x (Figs. 7a and 8a) and vertical component u_z (Figs. 7c and 8c) are very clear. The wave-field snapshots, generated by both the NADM and the ONADM, show that the ONADM has less numerical dispersions even if the space increment chosen is 50 m without any additional treatments. The computation to generate three-component

results in Figures 7 and 8 were performed on a Pentium 4 PC with 128MB RAM. The ONADM took about 3.4 min to generate Figure 8 while the original NADM took about 5 min to generate Figure 7. This coincides with our theoretical conclusion that the ONADM can save the computational cost about 32% compared with the NADM.

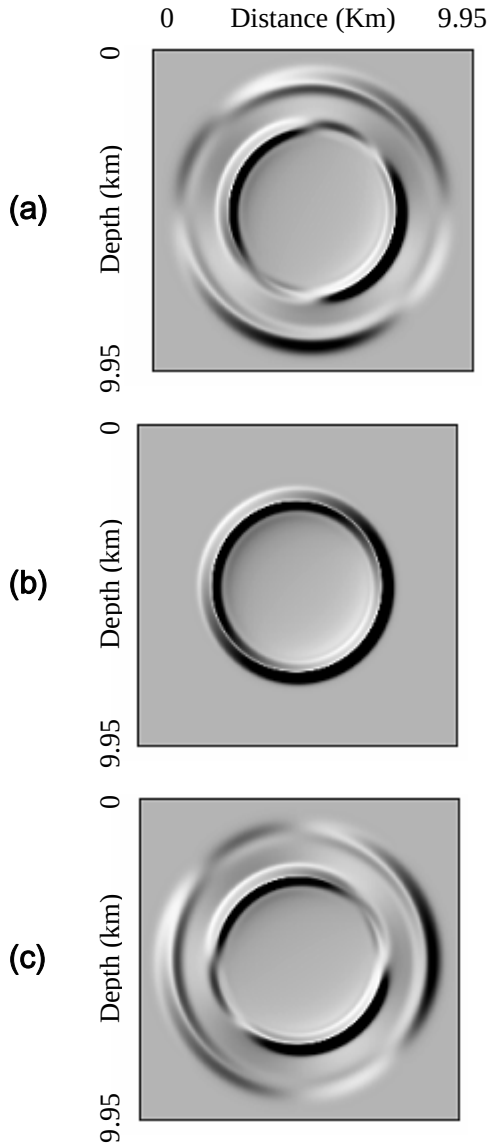

Figure 7. Snapshots of seismic wave fields for three-components at time 1.4 sec in isotropic media, generated by NADM, for (a) u_x component, (b) u_y component, (c) u_z component.

For further comparison, we present the waveforms computed using the NADM, the ONADM, and the second-order FD. In this model 2, we use the spatial step size $\Delta x = \Delta z = 20$ *m*, the time increment $\Delta t = 10^{-3}$ s, and the grid points 300×300. The

computational domain is chosen as $0 \le x \le 5.98$ km, $0 \le z \le 05.98$ km. The source is located at $(x_s, z_s) = (2$ km, 3 km) and the receiver is at $(x, z) = (3$ km, 3 km). The rest model parameters are same as those in model 1.

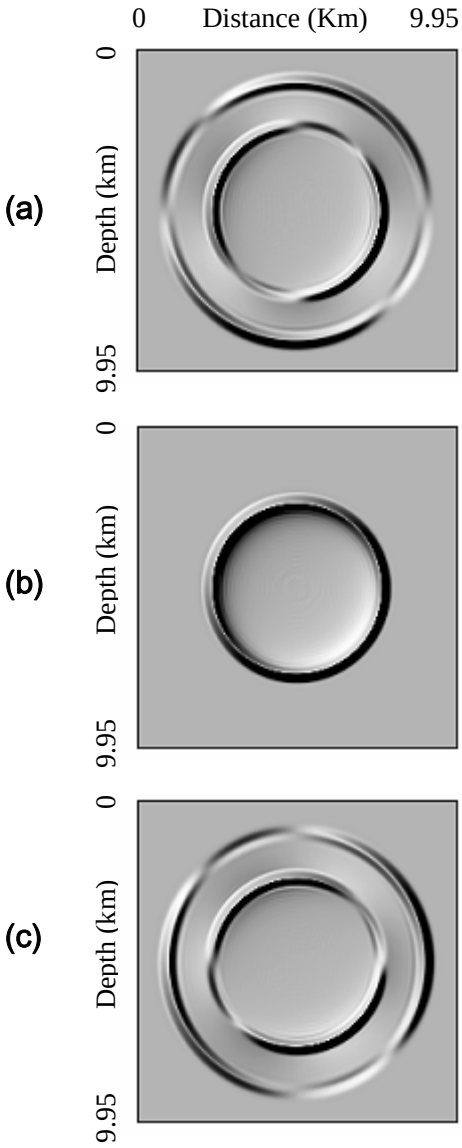

Figure 8. Snapshots of seismic wave fields for three-components at time 1.4 sec in isotropic media, generated by the ONADM, for (a) u_x component, (b) u_y component, (c) u_z component.

Figure 9 presents the waveforms of three components in the isotropic medium, generated by the NADM, the ONADM, and the second-order FD. Figures 9a and 9b show that the waveforms generated by the ONADM are identical with those computed by the NADM excepting for marginal difference behind wave peaks. However, the computational times required by the ONADM and the NADM are different. It took the

ONADM about 25 minutes CPU time to generate Figure 9b, while generating Figure 9a with the same conditions costs the NADM about 37 minutes. This also confirms our theoretical conclusions. Meanwhile, comparing Figures 9a and 9b with Figure 9c, we can observe that both the ONADM and the NADM have fairly less numerical dispersions while the second-order FD suffers from seriously numerical dispersions.

(a) NADM

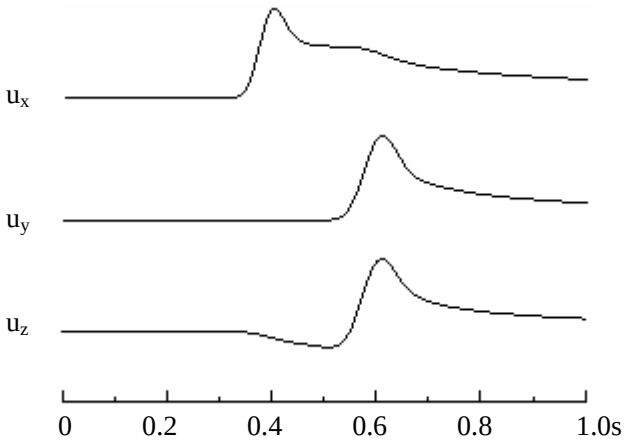

(b) ONADM

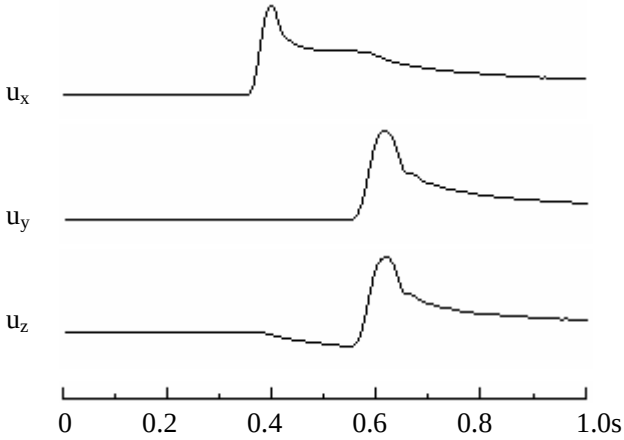

(c) Second-order FD

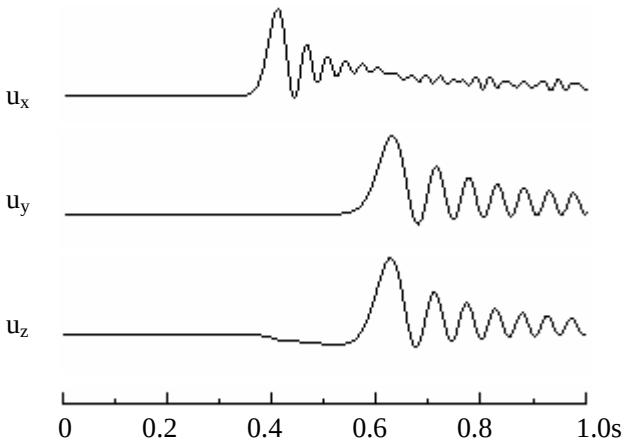

Figure 9. A comparison of the three-component waveforms in a homogeneous isotropic medium. The synthetic seismograms (a), (b), and (c) are generated by the NADM, the ONADM, and the second-order FD, respectively.

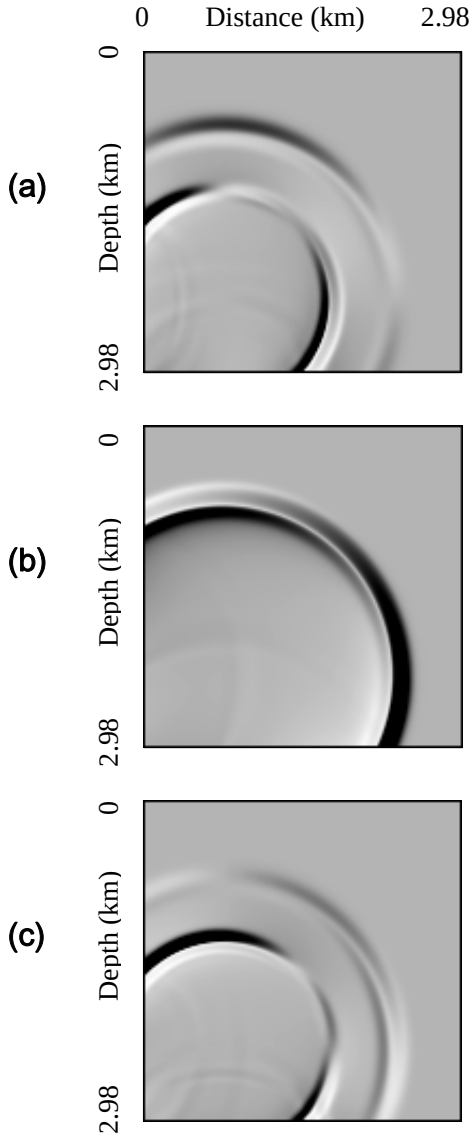

Figure 10. Snapshots of seismic wave fields for three components at time 0.61 sec for the u_x and u_z components and at time 0.95 sec for the u_y component in isotropic media, generated by the ONADM with the 4-times absorbing boundary condition.

The goal of the final example is to investigate the validity of the n-times decoupled absorbing condition (9) while incorporating the n-times absorbing boundary condition in the ONADM. In this model, we choose the absorbing boundary condition with orders of n=4 in equation (9). The computational domain is chosen as $0 \le x \le 2.98$ km, $0 \le z \le 2.98$ km. The source is located at (0.66 km, 2.24 km). The computational parameters are chosen by h=20 m, $\Delta t = 1.5 \times 10^{-3}$ sec, the number of grid points

150×150, and other parameters are the same as those used in model 1.

Figure 10 contains three-component snapshots, generated by the ONADM with the 4-times absorbing boundary condition. The wavefield snapshots (Figs. 10a and 10c) and the snapshot shown in Figure 10b are taken at propagation time 0.61 sec and 0.95 sec, respectively. From the wavefield snapshots, we can observe that the reflections of P- and S-waves from the artificial boundaries are effectively absorbed and the computation is stable. This illustrates that incorporating the 4-times absorbing boundary condition in the ONADM is effective.

Conclusions

We optimally modify the NADM, developed by Yang et al. (2003a) for solving acoustic and elastic wave equations. The optimal method enjoys 4-order accuracy in both space and time while the NADM has only 2-order accuracy in time and 4-order accuracy in space. This conclusion is also verified by our numerical experiments of computing the relative error E_r via formula (11) for 1-D case and formula (13) for 2-D case. Both the numerical errors produced by the ONADM and NADM are smaller than that based on the fourth-order Lax-Wendroff correction (Dablain, 1986) and the conventional second-order FD method. Compared with the original NADM, the ONADM does not involve to the so-called velocity $\overline{W}$. Therefore, it can substantially save storage, reduce the computational cost, and improve greatly the numerical accuracy. Our theoretical conclusions are verified by promising numerical results, which demonstrate that the optimal method can save computational costs-by about 32% and storage space-by about 53% as compared with the original NADM. Wave-field modeling also illustrates that the optimal method can effectively suppress numerical dispersions when too-coarse computation grids are used. This indicates that the optimal method enables wave propagation to be simulated in large-scale models through using the coarse computation grids. Besides, the numerical investigation of boundary conditions shows that the decoupling 4-times absorbing boundary condition, developed by Higdon (1991) and discretized by Yang et al. (2003b), works well.

Acknowledgments

We thank Johan O.A. Robertson for valuable comments that greatly contributed to improving the manuscript. We also thank Dr. Fred F. Pollitz (Associate Editor) for helpful comments. This work was supported by the National Natural Sciences Foundation of China (Grant No. 40174012) and the Foundation of Tsinghua University (Grant No. JC2002038). Part of this work was done when the first author visited Department of Computing and Software, McMaster University. This visit was partially supported by the MITACS project ``New interior point methods and software for convex conic linear optimization with applications to solving VLSI circuit layout problems". The research of the last author was partially supported by the grant #RPG 249635-02 of the National Sciences and Engineering Research Council of Canada (NSERC), a PREA award from Ontario, and the above-mentioned MITACS project.

References

Alford, R. M., K. R. Kelly, and D. M. Boore (1974). Accuracy of finite-difference modeling of the acoustic wave equation, *Geophysics* **39**, 834-842.

Blanch, J. O. and J. O. A. Robertsson (1997). A modified Lax-Wendroff correction for wave propagation in media described by Zener elements, *Geophys. J. Int*. **131**, 381-386.

Chew, W. C. and Q. H. Liu (1996). Perfectly matched layers for elastodynamics: A new absorbing boundary condition, *J. Computational Acoust*. **4**, 341-259.

Dablain, M. A. (1986). The application of high-order differencing to the scalar wave equation, *Geophysics* **51**, 54-66.

Fei, T. and K. Larner (1995). Elimination of numerical dispersion in finite-difference modeling and migration by flux-corrected transport, *Geophysics* **60**, 1830-1842.

Geller, R. J. and N. Takeuchi (1998). Optimally accurate second-order time-domain finite difference scheme for the elastic equation of motion: one-dimensional case, *Geophys. J. Int*. **135**, 48-62.

Higdon, R. L. (1991). Absorbing boundary conditions for elastic waves, *Geophysics* **56**, 231-241.

Igel, H., P. Mora, and B. Riollet (1995). Anisotropic wave propagation through finite-difference grids, *Geophysics* **60**, 1203-1216.

Kelly, K., R. Ward, S. Treitel, and R. Alford (1976). Synthetic seismograms: a finite-difference approach, *Geophysics* **41**, 2-27.

Konddoh Y., Y. Hosaka, and K. Ishii (1994). Kernel optimum nearly analytical discretization algorithm applied to parabolic and hyperbolic equations, *Computers Math. Appl.* **27**, 59-90.

Kosloff, D. and E. Baysal (1982). Forward modeling by a Fourier method, *Geophysics* **47**, 1402-1412.

Liu, Q. H. and J. Tao (1997). The perfectly matched layer for acoustic waves in absorptive media, *J. Acoust. Soc. Am*. **102**, 2072-2082.

Mizutani, H., R. J. Geller, and N. Takeuchi (2000). Comparison of accuracy and efficiency of time-domain schemes for calculating synthetic seismograms, *Phys. Earth Planet. Int.* **119**, 75-97.

Robertsson, J. O. A., J. O. Blanch and W. W. Symes (1994). Viscoelastic finite-difference modeling, *Geophysics* **59**, 1444-1456.

Takeuchi, N. and R. J. Geller (2000). Optimally accurate second order time-domain finite difference scheme for computing synthetic seismograms in 2-D and 3-D media, *Phys. Earth Planet. Int.* **119**, 99-131.

Virieux, J. (1986). P-SV wave propagation in heterogeneous media: Velocity-stress finite-difference method, *Geophysics* **51**, 889-901.

Wang, S. Q., D. H. Yang, and K. D. Yang (2002). Compact finite difference scheme for elastic equations, *J. Tsinghua Univ. (Sci. & Tech.)* **42**, 1128-1131. (in Chinese)

Yang, D. H., E. Liu, Z. J. Zhang, and J. Teng (2002). Finite-difference modelling in two-dimensional anisotropic media using a flux-corrected transport technique, *Geophys. J. Int*. **148**, 320-328.

Yang, D. H., J. W. Teng, Z. J. Zhang, and E. Liu (2003a). A nearly-analytic discrete method for acoustic and elastic wave equations in anisotropic media, *Bull. Seism.*

Soc. Am. **93**, 882-890.

Yang, D. H., S. Q. Wang, Z. J. Zhang, and J. W. Teng (2003b). n-times absorbing boundary conditions for compact finite difference modeling of acoustic and elastic wave propagation in the 2-D TI Medium, *Bull. Seism. Soc. Am.* **93**, 2389-2401.

Zahradnik, J., P. Moczo, and T. Hron (1993). Testing four elastic finite-difference schemes for behavior at discontinuities, *Bull. Seism. Soc. Am*. **83**, 107-129.

Zhang, Z. J., G. J. Wang, and J. M. Harris (1999). Multi-component wave-field simulation in viscous extensively dilatancy anisotropic media, *Phys. Earth Planet. Inter.* **114** 25-38.